BIOCHEMISTRY
including biophysical chemistry & molecular biology
Article

*Biochemistry* **2009,** *48,* 10733–10742 10733
DOI: 10.1021/bi900544p

# Helix Formation in Arrestin Accompanies Recognition of Photoactivated Rhodopsin[†,‡]

Sophie E. Feuerstein,[§,⊥] Alexander Pulvermüller,[@] Rudolf Hartmann,[§] Joachim Granzin,[∥] Matthias Stoldt,[§,⊥] Peter Henklein,[#] Oliver P. Ernst,[@] Martin Heck,[@] Dieter Willbold,[§,⊥] and Bernd W. Koenig*[,§,⊥]

[§]*Department Strukturbiochemie (ISB-3),* [∥]*Department Molekulare Biophysik (ISB-2) of the Institut für Strukturbiologie und Biophysik, Forschungszentrum Jülich, D-52425 Jülich, Germany,* [⊥]*Institut für Physikalische Biologie, Heinrich-Heine-Universität Düsseldorf, D-40225 Düsseldorf, Germany,* [@]*Institut für Medizinische Physik und Biophysik (CC2) and* [#]*Institut für Biochemie, Charité-Universitätsmedizin Berlin, Charitéplatz 1, D-10117 Berlin, Germany*

*Received March 31, 2009; Revised Manuscript Received October 16, 2009*

ABSTRACT: Binding of arrestin to photoactivated phosphorylated rhodopsin terminates the amplification of visual signals in photoreceptor cells. Currently, there is no crystal structure of a rhodopsin−arrestin complex available, although structures of unbound rhodopsin and arrestin have been determined. High-affinity receptor binding is dependent on distinct arrestin sites responsible for recognition of rhodopsin activation and phosphorylation. The loop connecting β-strands V and VI in rod arrestin has been implicated in the recognition of active rhodopsin. We report the structure of receptor-bound arrestin peptide Arr(67−77) mimicking this loop based on solution NMR data. The peptide binds photoactivated rhodopsin in the unphosphorylated and phosphorylated form with similar affinities and stabilizes the metarhodopsin II photointermediate. A largely α-helical conformation of the receptor-bound peptide is observed.

Numerous arrestins play a crucial role in regulation of signal transduction of G protein-coupled receptors (GPCRs),[1] while additional family members serve other functions (*1*). GPCR signaling is shut off by a conserved two-step process, i.e., phosphorylation of the GPCR followed by tight binding of arrestin. Four types of arrestin can be distinguished in vertebrates: rod arrestin (arrestin-1) and cone arrestin (arrestin-4) are restricted to the corresponding compartments of the retina, while nonvisual β-arrestin-1 (arrestin-2) and β-arrestin-2 (arrestin-3) are widely distributed in various tissues. In what follows, the term arrestin refers to bovine rod arrestin.

X-ray crystal structures are available for three arrestin subtypes, all of them reflecting the receptor-free form of the protein (*2*−*5*). The overall fold of the basal state of arrestin is conserved across the studied subtypes (*5*). However, the structure of arrestin in complex with its activated and phosphorylated GPCR remains elusive.

Uncomplexed arrestin has an elongated shape formed by two neighboring cuplike regions termed N- and C-domains (Figure 1). Each domain features a β-sheet sandwich that is stabilized by hydrophobic interactions. The N-domain contains an additional short helix (αI). The mutual arrangement of the N- and C-domains in the basal state of arrestin is determined mainly by two intramolecular linkers (Figure 1), the "polar core" (a salt bridge-stabilized network of residues D30, R175, D296, D303, and R382) (*6*) and the "three-element interaction region", which connects β-strand I and α-helix I of the N-domain with β-strand XX in the C-tail and is stabilized by hydrophobic interactions (*7*).

Arrestin preferentially binds light-activated phosphorylated rhodopsin (pRh*) with high affinity [$K_D \sim 50$ nM (*8*)], although low-affinity binding to unphosphorylated activated rhodopsin (Rh*) and to phosphorylated inactive ground state rhodopsin (pRh) has been reported (*9*−*11*). A sequential multisite binding model has been put forward for arrestin activation, implicating presumably separate "activation−recognition" and "phosphorylation−recognition" sites of arrestin that interact with the phosphorylated C-terminus and surface domains of the active metarhodopsin II (Meta II) conformation of the receptor, respectively (*9*, *10*). Engagement of both sensors by pRh* is required to induce a new arrestin conformation that binds the receptor with high affinity (*10*).

The loop connecting β-strands V and VI in the crystal structure of arrestin [PDB entries 1ayr (*2*) and 1cf1 (*3*)] has been identified as a major player in receptor activation−recognition (*11*−*15*). It encompasses residues Tyr67−Phe78 and is termed loop V−VI or the "finger loop" of arrestin (*11*). Insertion of 10-amino acid tags between either residues 72 and 73 or residues 77 and 78 of arrestin (*12*) as well as single-point mutations of loop residues (L77C, S78C, and F79C) significantly reduces the level of binding of arrestin to pRh* in comparison with that of wild-type

[†]This work was supported by grants from the Deutsche Forschungsgemeinschaft (DFG) to B.W.K. (Ko 2143/3), A.P. (Pu 186/3), and O.P.E. (Er 294/1).

[‡]The atomic coordinates, chemical shift assignments, and NOE-based structural restraints of Arr(67−77) in the Rh*-bound state (accession number 20079) have been deposited in the Biological Magnetic Resonance Data Bank and the Small Molecule Structure Deposition system.

*To whom correspondence should be addressed: ISB-3, Forschungszentrum Jülich, D-52425 Jülich, Germany. Phone: +49-2461-615385. Fax: +49-2461-618766. E-mail: b.koenig@fz-juelich.de.

[1]Abbreviations: GPCR, G protein-coupled receptor; Rh, bovine rhodopsin; Rh*, photoactivated Rh; pRh, phosphorylated Rh; pRh*, phosphorylated and photoactivated Rh; Arr(67−77), arrestin-derived peptide; Meta I, metarhodopsin I; Meta II, metarhodopsin II; pMeta II, phosphorylated Meta II; NOE, nuclear Overhauser effect; TrNOE, transferred NOE; ROS, rod outer segment of the retina; 2D, two-dimensional; $F_1$, indirect dimension in the 2D NMR spectrum; $F_2$, direct dimension in the 2D NMR spectrum; TOCSY, total correlation spectroscopy; ROESY, rotating frame nuclear Overhauser enhancement spectroscopy; FID, free induction decay; NOESY, nuclear Overhauser enhancement spectroscopy; $G_t$, G protein transducin; Ops*, $G_t$-binding state of opsin; $G_t\alpha(340-350)$, $G_t\gamma(50-71)$, and GαCT, transducin-derived peptides; PDB, Protein Data Bank; rmsd, root-mean-square deviation.


Published on Web 10/16/2009

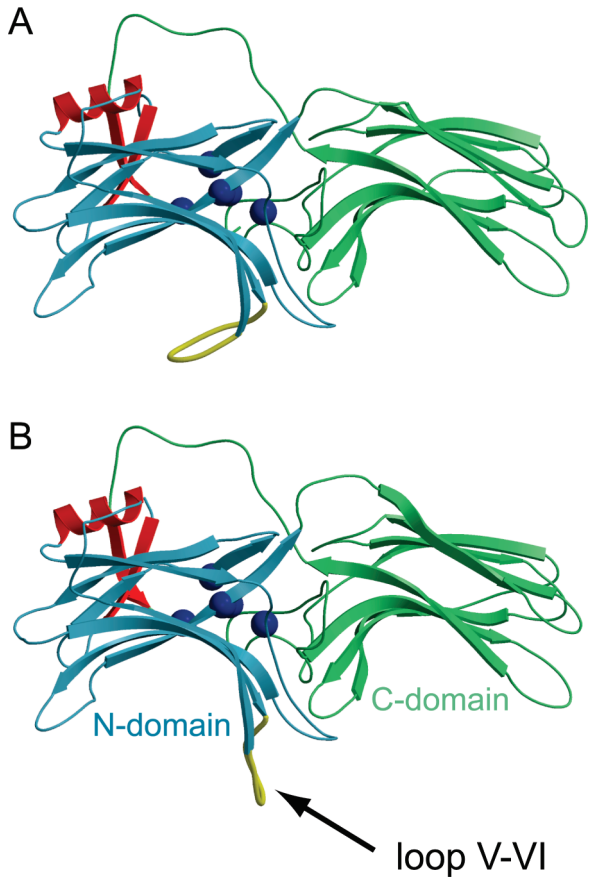


FIGURE 1: Crystallographic conformers of visual arrestin [refined structure based on PDB entry 1ayr (*2*) and unpublished results of J. Granzin]. Unbound arrestin features two $\beta$-sheet sandwiches, termed the N- and C-domains. Each sandwich displays one concave surface. Receptor-binding elements primarily map onto these concave sides (*10*). Arrestin is held in the basal state by two intramolecular interactions: (i) the polar core, a salt bridge-stabilized network of five charged amino acids (D30, R175, D296, D303, and R382, symbolized by blue spheres), and (ii) the three-element interaction involving $\beta$-strand I (arrestin residues 10−16), $\beta$-strand XX (residues 375−379), and α-helix I (residues 102−111) (colored red). Two distinct arrestin conformers are observed in the asymmetric unit cell of the protein crystal. The main structural difference between the two is the loop connecting $\beta$-strands V and VI (colored yellow) which is either folded toward the N-terminal domain (A, "closed" conformation) or extended away from the N-domain (B, "open" conformation).

arrestin (*11*). Spectroscopic properties of a cysteine-attached fluorescent dye in the single-cysteine mutant Arr(I72C) indicate burying of loop V−VI in the arrestin−rhodopsin interface (*13*, *14*). Likewise, spin-labels attached to cysteines in arrestin mutants I72C, V74C, and M75C exhibit high mobility in free arrestin but become essentially immobilized upon binding of arrestin to pRh*, again indicating embedding of loop V−VI in the arrestin−rhodopsin interface (*11*).

Despite a high degree of similarity between the X-ray structures of unbound arrestins from different subtypes (*2*−*5*, *16*), loop V−VI shows large variability. The two conformers seen in the asymmetric unit of bovine rod arrestin crystals (*2*, *3*) show two loop structures: a "closed" conformation where loop V−VI is in contact with the concave side of the N-domain and an "open" state where this loop points away from the arrestin surface (Figure 1) (*2*). Using a combination of cysteine mutagenesis and fluorescence quenching, Sommer et al. (*15*) showed that loop V−VI is at least temporarily close to the N-domain in unbound arrestin while upon pRh* binding is extended away from the arrestin surface and buried in the interface of the complex. Furthermore, restraining the conformational space of loop V−VI to a closed conformation abolishes pRh* binding (*15*). The structural flexibility of loop V−VI is apparently essential for the ability of arrestin to adopt a new conformation that is capable of high-affinity receptor binding.

The strong reduction in the mobility of loop V−VI upon pRh* binding does very likely reflect a well-defined conformation of the finger loop in the pRh*−arrestin complex. However, neither previous crystallographic nor spectroscopic studies give any indication on the detailed structure of this loop in the receptor-bound state. We used liquid state NMR to determine the high-resolution structure of the 11-residue peptide Arr(67−77), matching the amino acid sequence of loop V−VI, bound to the activated state of rhodopsin in native disk membranes.

## MATERIALS AND METHODS

*Peptide Synthesis*. Synthetic peptides were produced using Fmoc chemistry with HBTU activation in a model 433A peptide synthesizer (Applied Biosystems). Peptides were purified by reversed phase HPLC. Peptide purity (>98%) was confirmed by electrospray ionization mass spectrometry and finally NMR spectroscopy. The undecapeptide Arr(67−77) corresponds to amino acid residues 67−77 of bovine rod arrestin (YGQEDIDVMGL). A peptide exhibiting an amino acid composition identical to that of Arr(67−77) but a scrambled sequence (DMGVDEQLYIG) was used for control measurements.

*Disk Membrane Preparation*. Fresh bovine eyes were obtained from a local slaughterhouse (Viersen, Germany) and transported in a light-proof container. All procedures were conducted under dim red light. Samples were kept on ice, and tubes and solutions were chilled in ice buckets prior to use. Retinas were removed from the eyes within a few hours, shock frozen in liquid nitrogen, and stored at −80 °C. Retinal rod outer segments (ROS) were isolated by the discontinuous sucrose gradient method (*17*) and stored at −80 °C until they were used. Hypotonically stripped disk membranes were isolated from ROS by ficoll floatation in a manner similar to a published procedure (*18*) except that a lower ficoll concentration was used [2 or 3.5% (w/v) instead of 5%]. Disks were washed twice (48000*g* for 30 min at 4 °C) either in NMR buffer [10 mM sodium phosphate (pH 6.6) and 20 mM KCl] or in 100 mM HEPES (pH 8.0) (samples for spectrophotometry). This method yields osmotically intact disk membrane vesicles with a size larger than 400 nm. Finally, the suspension was forced through either 2 or 5 $\mu$m Nucleopore track-etched polycarbonate membranes (Whatman). This removes vesicle aggregates and results in isolated disks.

The rhodopsin concentration was derived from the absorption spectrum using an $\varepsilon_{500}$ of 40000 $M^{-1}$ $cm^{-1}$ (*19*). The purity of the disk membrane solution was confirmed on the basis of the $A_{280}/A_{500}$ spectral ratio (*20*) which was always between 1.7 and 2.0. Phosphorylated rhodopsin was prepared as described by Pulvermüller et al. (*21*). Membranes were kept on ice and used within 4 days without any loss of activity.

*NMR Sample Preparation*. Free peptide was studied at a concentration of 1 mM in NMR buffer containing 10 vol % $^2H_2O$. Rhodopsin-containing NMR samples were prepared under dim red light. The disk membrane suspension and peptide stock solution in NMR buffer were combined and supplemented with 10 vol % $^2H_2O$ to give 350 $\mu$L NMR samples containing

dark state rhodopsin (50 $\mu$M) and Arr(67−77) peptide (2 mM) at pH 6.6. Samples were transferred to Shigemi NMR microcells and inserted into the NMR magnet without being exposed to light.

NMR spectra of photoactivated samples were recorded after the NMR sample had been subjected for 30 s to intense white light sent through a Schott GG495 long-pass filter. The sample was re-inserted into the magnet immediately after light activation and briefly equilibrated at 10 °C. Data acquisition started ~2 min after photobleaching.

*NMR Experiments*. NMR data were recorded at 10 °C on Varian Unity INOVA 600 and 800 MHz spectrometers operating at 14.1 and 18.8 T, respectively. Triple-resonance 5 mm $^{1}$H-($^{13}$C,$^{15}$N) probes with actively shielded *z*-axis pulsed field gradient coils were used. At 18.8 T, an HCN cold probe with cryogenically cooled $^{1}$H coil and preamplifier circuitry was employed. The water signal was suppressed with the WATERGATE sequence (*22*) and convolution of time domain data (*23*). Quadrature detection in the indirect ($F_1$) dimension was accomplished utilizing the States method (*24*). Spectra were processed with either VNMR or NMRPipe (*25*).

Two-dimensional (2D) total correlation spectroscopy (TOCSY) and rotating frame nuclear Overhauser enhancement spectroscopy (ROESY) data sets of the free Arr(67−77) peptide were acquired at 14.1 T for proton resonance assignment. The T-ROESY variant was utilized which effectively removes unwanted TOCSY cross-peaks from ROESY spectra (*26*, *27*). Data matrices with 128 × 641 (TOCSY) and 128 × 1200 (T-ROESY) complex points in $F_1$ and $F_2$, respectively, were recorded with 32 (TOCSY) and 64 (T-ROESY) transients per free induction decay (FID). The spectral width was 6000 Hz in both dimensions. A 70 ms DIPSY spin-lock sequence at a RF field strength of 6 kHz was employed for mixing in TOCSY experiments. A 300 ms mixing time was applied in T-ROESY using the periodic multiple-pulse sequence of Hwang and Shaka (*26*) for spin-locking at a field strength of 5.2 kHz. Apodization was achieved with 90°-shifted sine-bell ($F_2$) and 90°-shifted squared sine-bell ($F_1$) window functions. Data matrices were zero-filled to 1024 × 2048 points.

Nuclear Overhauser enhancement spectroscopy (NOESY) data of Arr(67−77) in samples containing rhodopsin-rich disk membranes at 10 °C were measured at 18.8 T employing a mixing time ($\tau_{mix}$) of 33 ms. First, 10 2D NOESY spectra of the peptide were acquired with four transients per FID each in the presence of dark state rhodopsin. These spectra were averaged to improve the signal-to-noise ratio. Immediately after photoactivation of rhodopsin, four-transient NOESY (total measuring time of 52 min) was started employing the same sample and identical acquisition parameters; 256 × 1800 complex data points were recorded for each NOESY experiment, resulting in acquisition times of 28 ms ($F_1$) and 200 ms ($F_2$). Squared sine-bell window functions shifted by 83° ($F_1$) and 72° ($F_2$), respectively, were applied. Data sets were zero-filled to 1024 × 2048 points. Rh* converts into retinal-free opsin in an exponential fashion with a time constant of ~30 min (*28*). We measured similar time constants for the release of retinal in the presence (~30 min) and absence (~35 min) of Arr(67−77) at 10 °C and pH 6.6. The gradual decrease in the number of peptide-binding sites during NMR data acquisition results in slightly broadened NMR signals but has no effect on the relative intensity of NOESY cross-peaks.

*NOE-Based Distance Constraints*. NOESY cross-peak intensities were converted to $^{1}$H−$^{1}$H distance constraints assuming an $r^{-4}$ dependence, to minimize the effect of potential spin diffusion on derived distances *r* (*29*). The intensity−distance relationship was calibrated empirically by requesting that all derived sequential $d_{\alpha N}$ and $d_{NN}$ distances be within established limits based on known bond lengths in the protein backbone and sterically allowed values of backbone torsion angles (*30*). No distance constraints were derived from weak cross-peaks between protons A and B if strong cross-peaks from both A and B to a third proton C were present, a situation that might indicate spin diffusion. Distance limits of $r \pm 0.2r$ were utilized for backbone−backbone and backbone−side chain interactions, while $r \pm 0.3r$ was used for side chain−side chain NOEs for structure calculation.

*Structure Calculation*. An ab initio simulated annealing protocol was implemented in Xplor-NIH (*31*) for calculation of the Rh*-bound structure of Arr(67−77). Transferred NOE (TrNOE)-based distances were the only experimental constraints utilized in the restraint molecular dynamics calculation. Partial or complete overlap of some cross-peaks is a common challenge in 2D NOESY data. If the presence of a specific $^{1}$H−$^{1}$H NOE could clearly be deduced from the spectral data despite partial peak overlap, the NOE was treated as a unique distance constraint. However, an "or statement" was used for the definition of an ambiguous distance constraint if there was any doubt which NOEs were contributing to an overlaid cross-peak. In such or statements, all possible assignments of the observed cross-peak are considered. Sum averaging was applied in the calculation of the potential energy term reflecting the TrNOE-derived distances to account for ambiguous distance constraints (*32*). The force field was specified by all-hydrogen parameter and topology files parallhdg.pro and topallhdg.pro, respectively. A template structure was randomized in a high-temperature search stage ($T_{start}$ = 1000 K, 5000 steps, 5 fs each). Initial velocities were assigned to each atom from a Maxwell distribution using a random number seed (*33*). A set of 100 structures were refined in the subsequent cooling stage (5000 steps, 5 fs each, distributed over a 1000 to 100 K temperature ramp with a step size of 50 K) and finally energy minimized.

*Spectroscopic Analysis of Binding of a Peptide to Rhodopsin*. A two-wavelength UV 3000 (Shimadzu, Kyoto, Japan) spectrophotometer (2 nm slit width) equipped with thermostated cuvettes, temperature regulation, and a green photoflash (filtered to 500 ± 20 nm) was used to measure the differences in absorption at 380 nm (photoproduct Meta II) and 417 nm. The isosbestic point between Meta I and Meta II at 417 nm was used to subtract light scattering artifacts from the absorption signal (*8*).

When rhodopsin in its natural disk membrane environment is cooled to temperatures at which the equilibrium is on the Meta I side (pH 8.0 and < 5 °C) (*34*), specific binding of a protein or peptide to Meta II formed after a flash of light is seen as an increased yield of Meta II (extra Meta II). Extra Meta II provides a kinetic and stoichiometric monitor for the complex between photoactivated rhodopsin and the interactive polypeptide (*35*, *36*).

*Circular Dichroism Spectroscopy*. CD spectra of 46 $\mu$M Arr(67−77) in 10 mM sodium phosphate buffer (pH 7.0) were recorded at room temperature. Far-UV CD data were collected between 250 and 190 nm on a Jasco J-810 spectropolarimeter (Jasco, Tokyo, Japan) operating in continuous scan mode (scan speed of 20 nm/min, bandwidth of 1 nm, response time of 2 s, and accumulation of eight scans). A rectangular suprasil QS quartz

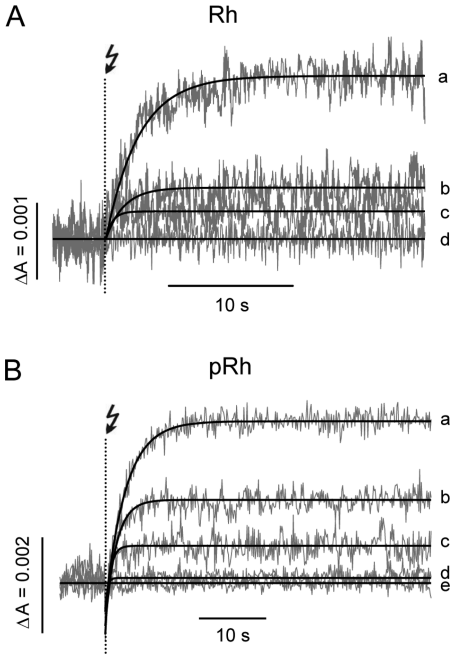


FIGURE 2: Flash-induced formation of extra Meta II in a suspension of washed disk membranes. The signals represent the absorbance change at 380 nm minus the absorbance change at 417 nm (see Materials and Methods). (A) Extra Meta II formation in unphosphorylated washed ROS membranes in the presence of (a) 6.6, (b) 1.9, (c) 1.0, and (d) 0 mM Arr(67−77) peptide. (B) Extra Meta II formation in phosphorylated washed ROS membranes in the presence of (a) 6.7, (b) 2.7, (c) 1.0, (d) 0.1, and (e) 0 mM Arr(67−77) peptide. In all measurements, the final rhodopsin concentration was 10 $\mu$M in 100 mM HEPES (pH 8.0) at 4 °C. The total sample volume was 200 $\mu$L, with a cuvette path length of 2 mm, and the flash photolyzed 19% of rhodopsin.

cell with an optical path length of 1 mm (Hellma, Müllheim, Germany) was used. Baseline scans of sodium phosphate buffer without protein were subtracted from the CD curves.

## RESULTS

*Arr(67−77) Stabilizes the Meta II Photoproduct*. The spectrophotometric data in Figure 2 show the flash-induced formation of Meta II for different concentrations of the arrestin peptide Arr(67−77) at a constant amount of unphosphorylated or phosphorylated ROS membranes, i.e., containing either unphosphorylated or phosphorylated rhodopsin. The records in Figure 2 demonstrate the enhanced formation of Meta II for unphosphorylated (Rh, panel A, traces a−d) and phosphorylated ROS membranes (pRh, panel B, traces a−e) in the presence of increasing Arr(67−77) concentrations.

The dissociation constants ($K_D$) of the interactions between Arr(67−77) and phosphorylated Meta II (pMeta II) or unphosphorylated Meta II were determined by the procedure introduced by Schleicher et al. (*8*). A similar algorithm had been applied in determining dissociation constants for the interactions of active rhodopsin with arrestin and p[44] (*37*) or with rhodopsin kinase (*38*) or of activated transducin ($G_t$) with the cognate effector, a cGMP specific phosphodiesterase (*39*). At a constant concentration of photolyzed rhodopsin and an increasing Arr(67−77) concentration, the extra Meta II signal amplitude increases (Figure 3). To fit the data, the mass action law was used with the conservation of the total amount of Meta II and Arr(67−77) (Figure 3A) or pMeta II and Arr(67−77) (Figure 3B). For the Meta II and Arr(67−77) interaction, the

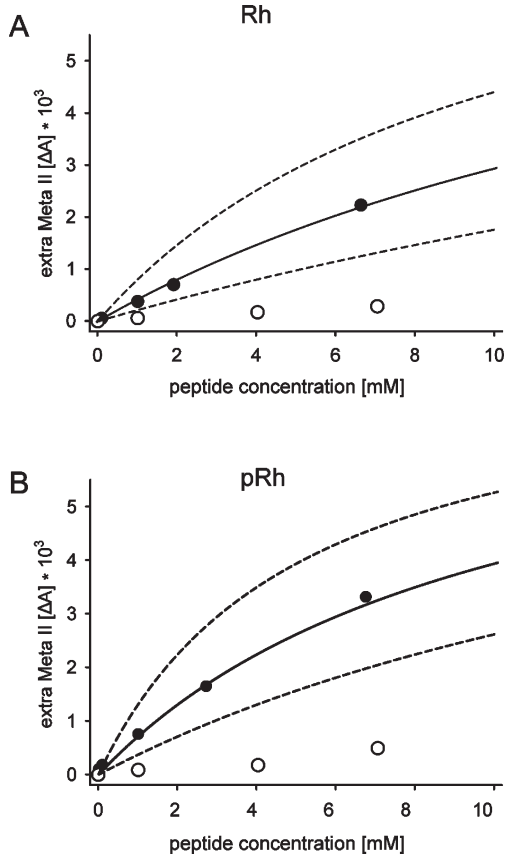


FIGURE 3: Extra Meta II formation induced by titration of rhodopsin with the Arr(67−77) peptide (●). Control titrations with a scrambled peptide sequence did not show any dose-dependent effect on Meta II formation (○). (A) Saturation of the Arr(67−77)-dependent extra Meta II formation in ROS membranes as a function of peptide concentration. The plot shows final amplitudes of the Arr(67−77)-dependent component of the difference absorption signals from a first flash on a fresh sample. The best-fit curve (thick line) of the experimental data yields a dissociation constant for the Rh*−Arr(67−77) interaction with a $K_D$ of 1.9 mM. The top and bottom dashed lines represent curves for $K_D$ values of 0.9 and 3.8 mM, respectively. (B) Saturation of the Arr(67−77)-dependent extra Meta II formation in phosphorylated ROS membranes as a function of peptide concentration. The best-fit curve (thick line) of the experimental data yields a dissociation constant for the pRh*−Arr(67−77) interaction with a $K_D$ of 1.0 mM. The top and bottom dashed lines represent curves for $K_D$ values of 0.5 and 2.0 mM, respectively. Experimental conditions are described in the legend of Figure 2.

$K_D$ value was 1.9 ± 0.2 mM, and for pMeta II and Arr(67−77), the $K_D$ value was 1.0 ± 0.3 mM. A peptide with a scrambled Arr(67−77) sequence exhibited no dose-dependent effect on Meta II formation (Figure 3). This finding demonstrates specific interaction of Arr(67−77) with both unphosphorylated and phosphorylated rhodopsin with a similar affinity.

*NMR Spectroscopy of Arr(67−77)*. All $^1$H resonances of the free peptide, except for the amide proton of the N-terminal Tyr67, were assigned on the basis of a "sequential walk" through the amide−aliphatic "fingerprint" regions of 2D TOCSY and T-ROESY spectra. Exclusively intraresidue and sequential cross-peaks were found in the 2D T-ROESY spectrum, indicating the conformational flexibility of free Arr(67−77).

Peptide resonance assignments were reviewed on the basis of 2D NOESY experiments recorded in the presence of dark state and light-activated rhodopsin. Most of the resonance positions remained almost unchanged ($\Delta\delta$ < 0.03 ppm) in all three cases,

Table 1: Resonance Assignments of Arr(67−77) Protons at 10 °C

| residue | $H^N$ | $H^\alpha$ | $H^\beta$ | others |
|---|---|---|---|---|
| Tyr67 | ND | 4.14 | 3.05 | $\delta$(2,6) 7.11, $\varepsilon$(3,5) 6.82 |
| Gly68 | 8.80 | 3.94, 3.86 | − | − |
| Gln69 | 8.55 | 4.21 | 2.07, 1.98 | $\gamma CH_2$ 2.32, $\varepsilon CH_3$ 7.71, 6.89 |
| Glu70 | 8.70 | 4.21 | 2.00, 1.98 | $\gamma CH_2$ 2.23 |
| Asp71 | 8.25 | 4.54 | 2.66, 2.54 | − |
| Ile72 | 7.93 | 4.06 | 1.82 | $\gamma CH_2$ 1.39, $\gamma CH_3$ 1.12, $\delta CH_3$ 0.84 |
| Asp73 | 8.42 | 4.57 | 2.66, 2.56 | − |
| Val74 | 8.06 | 4.07 | 2.12 | $\gamma CH_3$ 0.89, 0.80 |
| Met75 | 8.38 | 4.43 | 2.04 | $\gamma CH_2/\varepsilon CH_3$ 2.61, 2.51 |
| Gly76 | 8.36 | 3.93, 3.83 | − | − |
| Leu77 | 7.77 | 4.15 | 1.58, 1.53 | $\gamma$CH ND, $\delta CH_3$ 0.86, 0.81 |

the only exception being Tyr67 Hα ($\Delta\delta = -0.09$ ppm) and H$\beta$ ($\Delta\delta = -0.07$ ppm) that showed slightly stronger shifts upon addition of rhodopsin. Apparently, the peptide is in fast exchange on the chemical shift time scale between free and bound states. The large excess of peptide over the number of potential binding sites results in averaged chemical shifts close to the free peptide values. Proton resonances of Arr(67−77) measured at 10 °C in the presence of Rh* are listed in Table 1.

Weak intraresidue and sequential cross-peaks become visible in NOESY spectra of Arr(67−77) upon addition of dark state rhodopsin even with very short mixing times (53 and 33 ms). Most likely, there is superficial and perhaps unspecific binding of the peptide either to lipid molecules or to the inactive receptor at the cytoplasmic surface of the intact disk membrane. Importantly, the absence of medium-range NOEs suggests the lack of a defined peptide conformation. Subsequent photoactivation of rhodopsin causes dramatic changes in the 2D NOESY spectrum. Cross-peak intensities increase by a factor of 2−3 in a highly nonuniform manner at the expense of diagonal peaks, and numerous new medium-range cross-peaks appear (Figure 4). In addition, resonance broadening is observed.

Quantitative interpretation of TrNOE data in terms of a bound peptide conformation requires the absence of indirect cross-relaxation due to spin diffusion during the mixing time. Direct cross-relaxation is observed already at short mixing times, while indirect cross-relaxation between spins A and B via a third spin C occurs after a certain lag time. A series of preliminary NOESY spectra of Arr(67−77) were recorded in the presence of Rh* using mixing times of 33, 43, 53, 73, and 103 ms. In addition to the large number of cross-peaks detected at a $\tau_{mix}$ of 33 ms, an increasing number of other cross-peaks emerged with longer mixing times. Given the large size of the bound complex, the additional cross-peaks may result from spin diffusion. Therefore, only NOE spectra recorded with the shortest $\tau_{mix}$ of 33 ms were used to derive proton−proton distances from the NMR data. A side effect of the unusually short mixing time is contamination of NOESY correlations of protons connected by three covalent bonds with COSY-type contributions, which was particularly severe for intraresidue HN−Hα cross-peaks (Figure 4). Contaminated cross-peaks were not used for structure calculation.

*Unbound Arr(67−77) Is Unstructured.* CD spectra of free Arr(67−77) in phosphate buffer exhibit a strong negative band immediately below 200 nm and a mean residue ellipticity close to zero for wavelengths above ~215 nm (data not shown). Such CD spectra are typical for unordered proteins. This observation confirms the lack of a defined conformation of the free peptide, in agreement with the 2D T-ROESY cross-peak pattern.

*NMR Structure of Receptor-Bound Arr(67−77).* Although the NOESY spectrum recorded after photoactivation of rhodopsin is dominated by NOEs caused by efficient cross-relaxation in the Rh*-bound peptide, the spectrum results from rapid chemical exchange of the peptide among three states: (i) peptide bound to Rh*, (ii) peptide bound to disk membrane sites exposed already in the dark state, and (iii) free peptide. Given the large excess of peptide (2 mM) over Rh* ($< 50\ \mu$M) in the NMR sample, it is reasonable to assume that the equilibrium distribution between states ii and iii is largely unaffected by the small fraction of peptide that is bound to Rh* at any point in time. NOE intensities reflecting the Rh*-bound peptide correspond therefore in good approximation to the difference in the respective cross-peaks in NOESY spectra recorded after and prior to photoactivation of rhodopsin.

A difference NOE spectrum was obtained by subtraction of a scaled preactivation NOESY spectrum from a postactivation spectrum acquired with identical parameters on the same sample. The empirical scaling factor is $<1$ and accounts for peak broadening and strong intra- and intermolecular cross-relaxation of peptide spins in the photoactivated sample (*40*). Cross-peak intensities were derived either directly from the difference spectrum or from inspection of individual peaks in the two original NOESY experiments. In particular, for low-intensity peaks the latter treatment is preferable.

The NOESY cross-peak pattern of Rh*-bound Arr(67−77) is indicative of a helical conformation (Figure 5). The higher intensity of $d_{NN}$ in comparison with $d_{\alpha N}$ cross-peaks and the presence of $d_{\alpha N}(i, i+3)$, $d_{\alpha\beta}(i, i+3)$, and $d_{NN}(i, i+2)$ NOE correlations are hallmarks of helices. The ambiguous nature of a fraction of the observed medium-range NOEs prohibits the determination of the helix extension directly from the NOE pattern.

A molecular dynamics-based simulated annealing protocol was used for calculation of Arr(67−77) conformations that satisfy the 154 experimental $^1H-^1H$ distance constraints [66 sequential, 29 ($i$, $i+2$), 39 ($i$, $i+3$), 18 ($i$, $i+4$), and 2 ($i$, $i+5$) constraints]. Twenty-six of these 154 distance constraints are ambiguous due to cross-peak overlap. Of the 100 structures calculated, the 20 peptide conformations with the lowest total energy were selected for analysis. An overlay of these 20 peptide structures is shown in Figure 6. Structural statistics for the ensemble are summarized in Table 2. The large majority of NOE distance constraints are satisfied in these structures; all remaining violations are $<0.3$ Å. The geometric quality of the calculated low-energy conformers was assessed with MolProbity (*41*). Eighty-five percent of the analyzed residues are found in favored regions and the remaining 15% in additionally allowed regions of the Ramachandran plot. The root-mean-square difference between the non-hydrogen atoms of the 20 simulated annealing structures and the mean structure amounts to 0.40 Å (backbone only) and 0.96 Å (including side chains). Analysis of the lowest-energy structures with DSSP (*42*) reveals three consecutive four-turn backbone hydrogen bonds [−CO($i$) to −NH ($i+4$)] from Gln69−Asp71 to Asp73−Met75. In the notation of Kabsch and Sander (*42*), this reflects an α-helix extending from Glu70 to Val74 (Figure 7). Backbone torsion angles $\phi$ and $\psi$ of

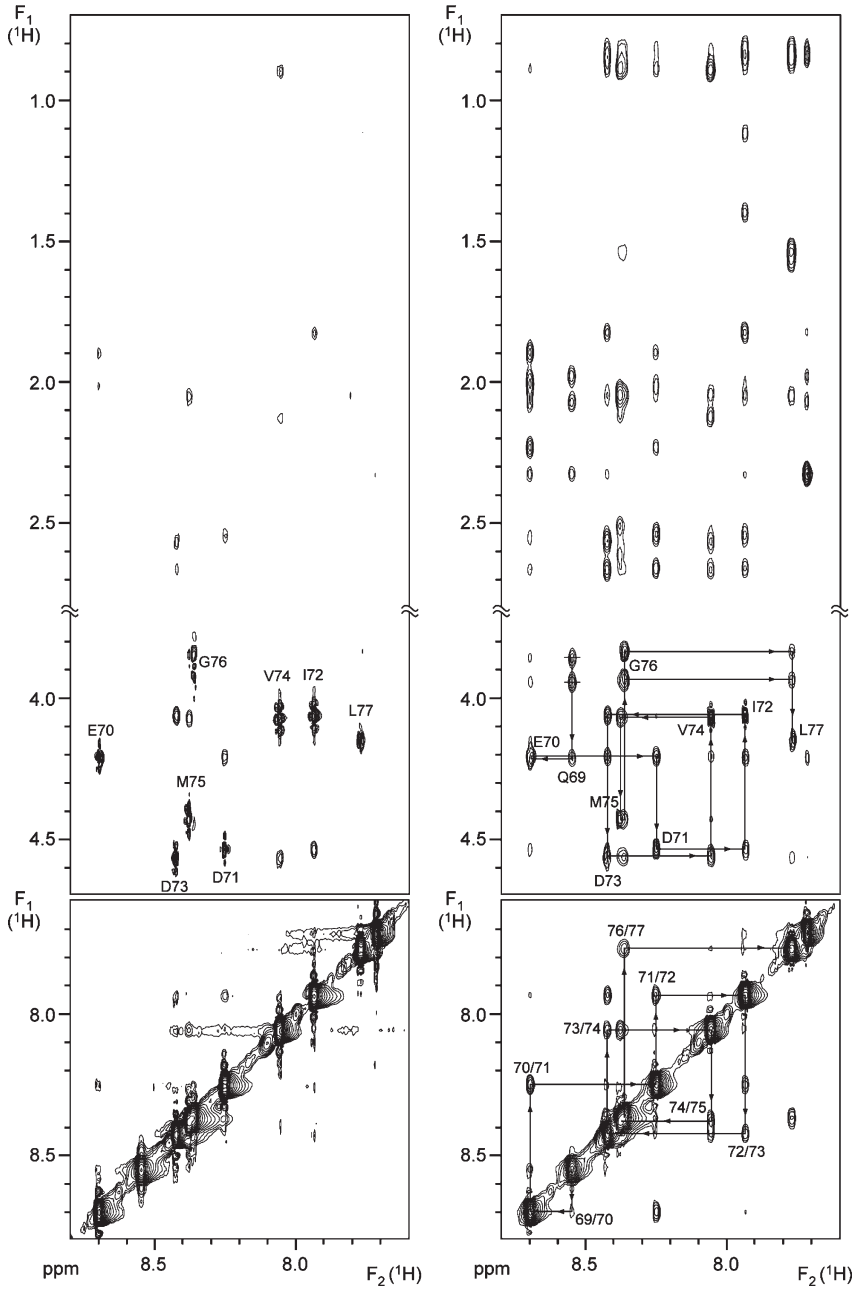


FIGURE 4: Selected regions of 2D NOESY spectra of Arr(67−77) in the presence of dark state (left) and photoactivated rhodopsin (right). Both the $H^N-H^N$ (bottom panels) and the $H^N$−aliphatic (fingerprint) regions (top panels) are shown. Exclusively intraresidue and weak sequential NOEs are observed in the dark state sample, indicating the lack of a unique peptide conformation. Correlations between vicinal protons, particularly the labeled $H^N-H^\alpha$ cross-peaks, display significant COSY contributions in the dark state resulting from the short mixing time. Photoactivation of rhodopsin causes a strong increase in both the number and intensity of observable cross-peaks. In particular, strong sequential $d_{NN}$ NOEs (labeled by residue numbers in the bottom right panel) and the appearance of nonsequential correlations reflect the formation of a preferred peptide conformation in the Rh*-bound state. Proton resonance assignment is based on a "sequential walk" (*30*) connecting intraresidue $H^N-H^\alpha$ (labeled) and sequential $d_{\alpha N}$ NOEs by a continuous path as illustrated in the top right panel.

residues 70−75 have values typically observed for right-handed helices.

Does phosphorylation of the receptor change the structure of the bound peptide? Additional NOESY spectra of Arr(67−77) were recorded in the presence of phosphorylated rhodopsin, both prior to and after photoactivation. The resulting spectra of Arr(67−77) are nearly identical to those obtained with unphosphorylated rhodopsin (Supporting Information). Helix specific NOEs are observed in both samples after photoactivation. No medium-range NOEs are detected prior to activation. The few differences between the two spectra acquired with either Rh* or pRh* are limited to the three N-terminal amino acids. We conclude that binding of Arr(67−77) to the activated receptor induces helix formation in a manner independent of receptor phosphorylation. However, the structure and/or dynamics of the N-terminus of the peptide may be sensitive to phosphorylation.

The cartoon of a modified arrestin structure in Figure 7A demonstrates the local structure change observed in loop V−VI upon receptor binding. Loop residues 67−77 of the arrestin crystal structure (Figure 1B) have been replaced by the NMR structure of bound Arr(67−77) followed by energy minimization. The designed structure exhibits reasonable geometry. Amino acid residues 55−90, covering $\beta$-stands V and VI and the connecting loop, do not show any steric overlap. All residues are in favored

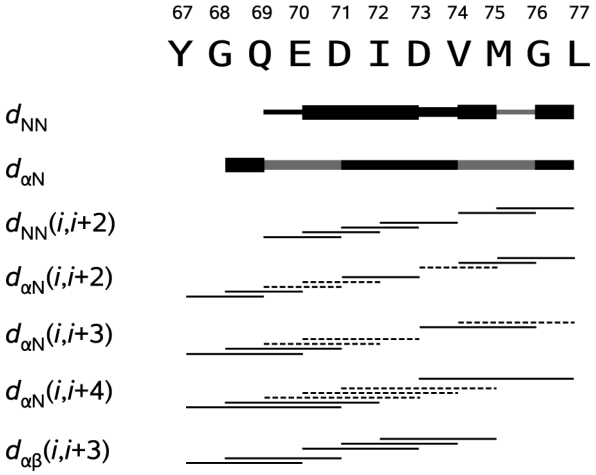


FIGURE 5: Summary of $^1H-^1H$ NOEs observed in the difference NOESY spectrum of Arr(67−77) reflecting the Rh*-bound peptide conformation. The thickness of the black lines in the top two rows is proportional to the intensity of the $d_{NN}$ and $d_{\alpha N}$ cross-peaks. Gray boxes indicate peaks that are definitely present but in which the peak intensity is affected by spectral overlap. The observation of medium-range NOEs is reflected in the bottom five rows. Dotted lines indicate cross-peak ambiguity due to peak overlap. The cross-peak pattern suggests the presence of a helical structure at least for part of the peptide sequence.

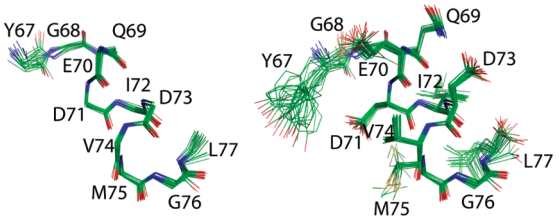


FIGURE 6: Superposition of the 20 lowest-energy structures of the Rh*-bound Arr(67−77) peptide. Bonds connecting non-hydrogen atoms in the backbone (left) and throughout the peptide (right) are represented by sticks. Atoms are colored green (carbon), red (oxygen), blue (nitrogen), and yellow (sulfur). The overlay is based on minimization of the rmsd between non-hydrogen atoms.

(77%) or allowed regions (23%) of the Ramachandran plot. Apparently, a helical structure of loop V−VI could be reconciled with nearby elements found in the crystal structure of uncomplexed arrestin.

## DISCUSSION

Arr(67−77) is unstructured in the absence of photoactivated rhodopsin. Activation causes conformational changes in rhodopsin (*43*, *44*) that apparently expose a binding site previously inaccessible for the Arr(67−77) peptide. Observation of a short α-helix ranging from Glu70 to Val74 (EDIDV) of the peptide sequence upon Rh* binding was rather unexpected. Of the five residues forming the helix, only Glu has a conformational preference for α-helices (Figure 7B), Ile and Val favor extended *β*-strands, and Asp is preferentially found in turn regions based on statistical analysis of protein crystal structures (*45*). The intermolecular interaction between Rh* and the peptide apparently provides a crucial helix stabilization that is absent prior to light activation of rhodopsin. Taking into account the formation of extra Meta II in the presence of the peptide, we conclude that Arr(67−77) specifically binds to the Meta II photoproduct.

A high Arrhenius activation energy observed upon binding of arrestin to phosphorylated Meta II suggests a substantial

Table 2: Structural Statistics for the 20 Lowest-Energy Structures of Rh*-Bound Arr(67−77)

| | |
|---|---|
| number of experimental restraints | |
| total number of NOE restraints | 154 |
| sequential | 66 |
| medium-range ($2 \leq \|i-j\| \leq 5$) | 88 |
| long-range ($\|i-j\| > 5$) | 0 |
| number of distance restraint violations (>0.3 Å) | none |
| rmsd from experimental distance restraints (Å) | 0.056 ± 0.001 |
| rmsd from idealized covalent geometry | |
| bonds (Å) | 0.0039 ± 0.0001 |
| angles (deg) | 0.67 ± 0.01 |
| impropers (deg) | 0.48 ± 0.02 |
| Xplor potential energies (kcal/mol) | |
| total | 52.3 ± 0.8 |
| bonds | 2.5 ± 0.1 |
| angles | 20.5 ± 0.7 |
| impropers | 2.9 ± 0.2 |
| van der Waals | 4.1 ± 0.5 |
| NOE | 22.3 ± 1.0 |
| rmsd from mean structure (backbone only/all heavy atoms) | |
| Arr(67−77) (Å) | 0.40/0.96 |
| Arr(68−76) (Å) | 0.15/0.67 |
| Ramachandran analysis | |
| favored region (%) | 85 |
| allowed region (%) | 15 |
| outlier region (%) | 0 |

conformational rearrangement of arrestin in the complex (*8*). Unfortunately, a crystal structure of the pMeta II−arrestin complex is still out of reach. The transient nature of the arrestin-binding Meta II photointermediate of the receptor presents a major obstacle for crystallization of the functional complex. The limited lifetime of the complex also impedes alternative structure determination techniques requiring extended data acquisition periods, like solid state NMR. Solution NMR faces the additional problem of the large rotational correlation time of membrane-anchored protein complexes, which prohibits acquisition of high-resolution NMR spectra. However, exchange-based liquid state NMR techniques present a viable alternative to this dilemma (*46*−*48*). The exchange-transferred nuclear Overhauser effect (TrNOE) allows structure determination of macromolecule- or membrane-bound small ligands on the basis of solution NMR data (*49*, *50*). For example, a membrane-embedded GPCR could represent the macromolecule, while a peptide corresponding to the receptor-binding domain of its interaction partner serves as a small ligand (*51*). Exchange-based solution NMR affords at least partial insight into the atomistic structure of membrane protein complexes in their native membrane environment (*40*, *52*). The relatively high sensitivity of exchange-based NMR methods enables rapid acquisition of two-dimensional NMR spectra. A detailed peptide structure can be derived from such data despite the limited lifetime of the peptide-binding Meta II photoproduct (*40*).

NOE experiments rely on cross-relaxation between protons that are close to each other in space. Cross-relaxation is much more efficient between protons in macromolecular complexes than in small ligands rapidly reorienting in solution with a rotational correlation time close to the value where the NOE undergoes a zero crossing (*47*). NOESY spectra of small peptides in fast exchange between a complex-bound and free form are

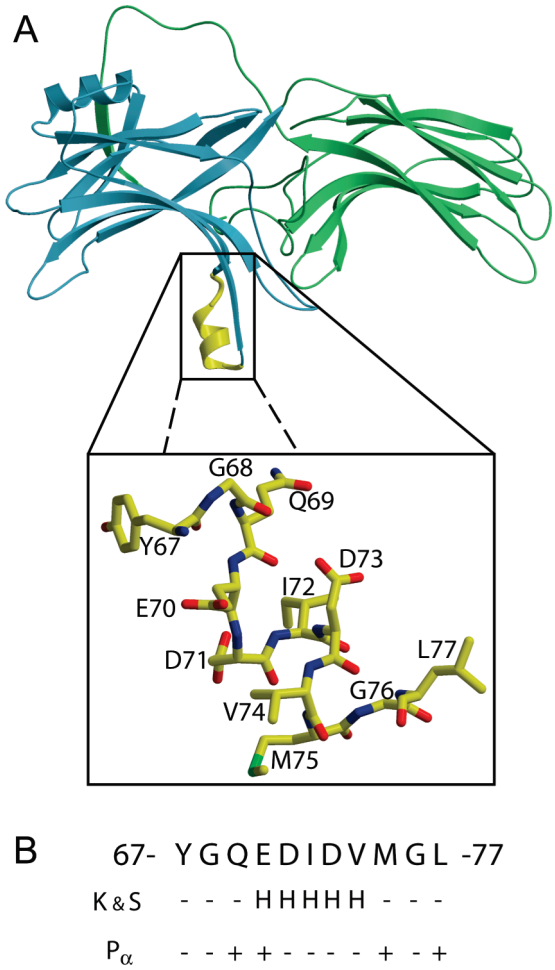


FIGURE 7: Arrestin loop V−VI adopts an α-helical structure upon binding Meta II. (A) Loop residues 67−77 in the open conformation of arrestin (Figure 1B) have been replaced by the NMR structure of Meta II-bound peptide Arr(67−77) followed by energy minimization. The close-up shows the peptide structure in a stick representation. Carbon (yellow), oxygen (red), nitrogen (blue), and sulfur atoms (green) are color-coded. (B) Shown is the amino acid sequence of Arr(67−77) (above). Residues in the NMR structure of Arr(67−77) that fulfill the criteria of an α-helix as defined by Kabsch and Sander (*42*) are indicated by the letter H (middle). The statistical propensity of individual amino acid types for helical structures (*45*) is denoted by a plus sign (below). All structure representations were produced with MOLSCRIPT (*64*) and RASTER3D (*65*) using secondary structure assignments generated by DSSP (*42*).

dominated by cross-relaxation in the bound state, provided the dissociation rate constant, $k_{off}$, is large compared to the rates of both cross-relaxation in the bound state and longitudinal relaxation of peptide nuclear spins; i.e., $k_{off}$ must be on the order of 1000 $s^{-1}$ or faster (*47*). Under these conditions, the observed TrNOEs reflect the structure of the bound peptide.

TrNOE data have been used previously for characterization of the arrestin-bound structure of phosphorylated peptides representing the C-terminus of rhodopsin (*53*, *54*) and of the G protein-coupled cannabinoid receptor (*55*). In addition, the Meta II-bound conformation of peptides reflecting the extreme C-terminus of the α- and γ-subunits of the heterotrimeric G protein transducin has been determined on the basis of TrNOE data (*52*, *56*) and from a combination of transferred dipolar couplings and TrNOEs (*40*). Interestingly, all those peptides are unstructured in solution and the corresponding regions in the uncomplexed parent protein are mostly disordered in the available X-ray structures. The observed bound peptide structure is apparently imposed by the interaction with the complementary binding partner.

Opsin is the ligand-free form of the GPCR rhodopsin. Recently, the crystal structure of a presumably active opsin conformation (Ops*) was published (*57*). The structure of uncomplexed Ops* is very similar to the crystal structure of opsin in its G protein-interacting conformation determined shortly thereafter (*58*). In the latter study, opsin was cocrystallized with the 11-residue peptide GαCT ($^{340}$ILENLKDCGLF$^{350}$), closely resembling the amino acid sequence of the $G_t\alpha$ C-terminus, which is the main receptor-binding site of $G_t$. Ops* binding induces a largely α-helical conformation of the GαCT peptide that is almost identical to the earlier TrNOE-based NMR structure of Rh*-bound $G_t\alpha$(340−350) (*52*). Moreover, the angle of the helical axis of GαCT with respect to the membrane normal in the crystal structure is in good agreement with the orientation of the bound peptide conformation previously determined from NMR-derived transferred dipolar couplings (*40*). The new X-ray data nicely reconfirm the power of exchange-based liquid state NMR techniques for structure determination of receptor-bound ligands.

The structural flexibility of loop V−VI in free arrestin (*2*, *11*, *15*) is an important aspect of receptor−arrestin recognition. Very likely, loop V−VI of uncomplexed arrestin samples a large number of different conformations. In the presence of light-activated rhodopsin, the helical conformation of the Arr(67−77) peptide is apparently selected from a diverse ensemble of conformations for specific binding to Meta II. Transferred NOEs are ideally suited for determination of the bound peptide structure. Recently, it was demonstrated that the recognition dynamics of ubiquitin, which binds a broad variety of different targets, is governed by conformational selection; i.e., all crystallographic structures of the ubiquitin interface in protein complexes observed previously are present in the conformational ensemble of the uncomplexed protein (*59*). We envision a similar recognition mechanism in the case of binding of arrestin loop V−VI to activated rhodopsin.

Modzelewska and co-workers compared four conceptual models of potential rhodopsin−arrestin complexes (*60*). They discussed binding of pRh* as a monomer to the concave surface of either the N- or C-domain or to the flap of arrestin that is located halfway between the N- and C-domain cavities. This protrusion includes the finger loop and extends away from the arrestin surface. Modzelewska and co-workers favor a model in which arrestin binds a rhodopsin dimer, arguing that the 2:1 stoichiometry produces the highest favorable interaction energy and buries the largest contact area (*60*). Among the three 1:1 models, binding of rhodopsin to the highly positively charged concave face of the N-domain produces the largest contact area surface and most favorable energy of interaction, closely followed by the model, in which rhodopsin binds to the central flap between the N- and C-domains (*60*). Recent experimental data suggest a 1:1 stoichiometry of the rhodopsin−arrestin complex. Hanson et al. used biochemical methods (*61*) as well as site-directed spin labeling and double electron−electron resonance spectroscopy (*62*) to demonstrate that only arrestin monomers bind phosphorylated photoactivated rhodopsin. Skegro et al. delineated the rhodopsin-binding region on the arrestin surface (*63*). Bulky fluorescence labels were introduced at the concave side of either the N- or C-terminal domain or to both regions simultaneously to sterically block local protein

interactions (*63*). Interestingly, tethering a single Alexa 633 fluorescence dye either to the N-domain or to the C-domain of arrestin did not compromise the arrestin−rhodopsin interaction at all. Introduction of two dye molecules, i.e., one into each of the two concave regions of arrestin, reduced the level of rhodopsin binding by ~50% in comparison with that of the unlabeled protein. However, tethering two dye molecules to each of the two concave regions of arrestin completely eliminated rhodopsin binding (*63*). These sterical blocking data are compatible with binding of activated rhodopsin in a 1:1 stoichiometry to the central protrusion between the two cavities of arrestin, i.e., one of the energetically favorable scenarios considered by Modzelewska et al. (*60*). This binding model could easily account for the major role of loop V−VI of arrestin in rhodopsin binding (*11*−*15*).

Our binding studies indicate that Arr(67−77) binds to and stabilizes the Meta II photoproduct. We speculate that the α-helical conformation of the Meta II-bound peptide reflects the conformation of the corresponding finger loop region in the arrestin−pRh* complex. Receptor binding of Arr(67−77) strictly requires rhodopsin activation but is rather insensitive to receptor phosphorylation. These observations support the sequential multisite binding model of receptor−arrestin interaction proposed by Gurevich and Gurevich (*10*) and suggest a crucial role of arrestin loop V−VI in the recognition of active rhodopsin.

## ACKNOWLEDGMENT

We thank Doris Höppner-Heitmann, Rudi Esser, and Ingrid Semjonow for expert assistance with the rhodopsin preparation, Martha Sommer, Darko Skegro, Thomas Stangler, and Oliver Weiergräber for helpful discussions, and Georg Büldt and Klaus Peter Hofmann for continuous support and interest.

## SUPPORTING INFORMATION AVAILABLE

Fingerprint region of the 2D TOCSY spectrum of Arr(67−77) (Figure S1), sections of 2D NOE spectra of Arr(67−77) recorded in the presence of Rh* and pRh* (Figure S2), and a close-up view of $d_{\alpha N}(i, i+4)$ NOEs of Arr(67−77) observed in the presence of Rh* (Figure S3). This material is available free of charge via the Internet at http://pubs.acs.org.

## REFERENCES

1. Xiao, K., McClatchy, D. B., Shukla, A. K., Zhao, Y., Chen, M., Shenoy, S. K., Yates, J. R.III, and Lefkowitz, R. J. (2007) Functional specialization of β-arrestin interactions revealed by proteomic analysis. *Proc. Natl. Acad. Sci. U.S.A. 104*, 12011–12016.
2. Granzin, J., Wilden, U., Choe, H. W., Labahn, J., Krafft, B., and Büldt, G. (1998) X-ray crystal structure of arrestin from bovine rod outer segments. *Nature 391*, 918–921.
3. Hirsch, J. A., Schubert, C., Gurevich, V. V., and Sigler, P. B. (1999) The 2.8 Å crystal structure of visual arrestin: A model for arrestin's regulation. *Cell 97*, 257–269.
4. Han, M., Gurevich, V. V., Vishnivetskiy, S. A., Sigler, P. B., and Schubert, C. (2001) Crystal structure of β-arrestin at 1.9 Å: Possible mechanism of receptor binding and membrane translocation. *Structure 9*, 869–880.
5. Sutton, R. B., Vishnivetskiy, S. A., Robert, J., Hanson, S. M., Raman, D., Knox, B. E., Kono, M., Navarro, J., and Gurevich, V. V. (2005) Crystal structure of cone arrestin at 2.3 Å: Evolution of receptor specificity. *J. Mol. Biol. 354*, 1069–1080.
6. Vishnivetskiy, S. A., Paz, C. L., Schubert, C., Hirsch, J. A., Sigler, P. B., and Gurevich, V. V. (1999) How does arrestin respond to the phosphorylated state of rhodopsin? *J. Biol. Chem. 274*, 11451–11454.
7. Vishnivetskiy, S. A., Schubert, C., Climaco, G. C., Gurevich, Y. V., Velez, M. G., and Gurevich, V. V. (2000) An additional phosphate-binding element in arrestin molecule. Implications for the mechanism of arrestin activation. *J. Biol. Chem. 275*, 41049–41057.
8. Schleicher, A., Kühn, H., and Hofmann, K. P. (1989) Kinetics, binding constant, and activation energy of the 48-kDa protein-rhodopsin complex by extra-metarhodopsin II. *Biochemistry 28*, 1770–1775.
9. Gurevich, V. V., and Benovic, J. L. (1993) Visual arrestin interaction with rhodopsin. Sequential multisite binding ensures strict selectivity toward light-activated phosphorylated rhodopsin. *J. Biol. Chem. 268*, 11628–11638.
10. Gurevich, V. V., and Gurevich, E. V. (2004) The molecular acrobatics of arrestin activation. *Trends Pharmacol. Sci. 25*, 105–111.
11. Hanson, S. M., Francis, D. J., Vishnivetskiy, S. A., Kolobova, E. A., Hubbell, W. L., Klug, C. S., and Gurevich, V. V. (2006) Differential interaction of spin-labeled arrestin with inactive and active phosphorhodopsin. *Proc. Natl. Acad. Sci. U.S.A. 103*, 4900–4905.
12. Dinculescu, A., McDowell, J. H., Amici, S. A., Dugger, D. R., Richards, N., Hargrave, P. A., and Smith, W. C. (2002) Insertional mutagenesis and immunochemical analysis of visual arrestin interaction with rhodopsin. *J. Biol. Chem. 277*, 11703–11708.
13. Smith, W. C., Dinculescu, A., Peterson, J. J., and McDowell, J. H. (2004) The surface of visual arrestin that binds to rhodopsin. *Mol. Vision 10*, 392–398.
14. Sommer, M. E., Smith, W. C., and Farrens, D. L. (2005) Dynamics of arrestin-rhodopsin interactions: Arrestin and retinal release are directly linked events. *J. Biol. Chem. 280*, 6861–6871.
15. Sommer, M. E., Farrens, D. L., McDowell, J. H., Weber, L. A., and Smith, W. C. (2007) Dynamics of arrestin-rhodopsin interactions: Loop movement is involved in arrestin activation and receptor binding. *J. Biol. Chem. 282*, 25560–25568.
16. Milano, S. K., Pace, H. C., Kim, Y. M., Brenner, C., and Benovic, J. L. (2002) Scaffolding functions of arrestin-2 revealed by crystal structure and mutagenesis. *Biochemistry 41*, 3321–3328.
17. Papermaster, D. S. (1982) Preparation of retinal rod outer segments. *Methods Enzymol. 81*, 48–52.
18. Smith, H. G., and Litman, B. J. (1982) Preparation of osmotically intact rod outer segment disks by ficoll flotation. *Methods Enzymol. 81*, 57–61.
19. Wald, G. (1968) The molecular basis of visual excitation. *Nature 219*, 800–807.
20. Smith, H. G., Stubbs, G. W., and Litman, B. J. (1975) The isolation and purification of osmotically intact discs from retinal rod outer segments. *Exp. Eye Res. 20*, 211–217.
21. Pulvermüller, A., Schröder, K., Fischer, T., and Hofmann, K. P. (2000) Interactions of metarhodopsin II. Arrestin peptides compete with arrestin and transducin. *J. Biol. Chem. 275*, 37679–37685.
22. Piotto, M., Saudek, V., and Sklenar, V. (1992) Gradient-tailored excitation for single-quantum NMR spectroscopy of aqueous solutions. *J. Biomol. NMR 2*, 661–665.
23. Marion, D., Ikura, M., and Bax, A. (1989) Improved solvent suppression in one- and two-dimensional NMR spectra by convolution of time-domain data. *J. Magn. Reson. 84*, 425–430.
24. States, D. J., Haberkorn, R. A., and Ruben, D. J. (1982) A two-dimensional nuclear Overhauser experiment with pure absorption phase in four quadrants. *J. Magn. Reson. 48*, 286–292.
25. Delaglio, F., Grzesiek, S., Vuister, G. W., Zhu, G., Pfeifer, J., and Bax, A. (1995) NMRPipe: A multidimensional spectral processing system based on UNIX pipes. *J. Biomol. NMR 6*, 277–293.
26. Hwang, T. L., and Shaka, A. J. (1992) Cross relaxation without TOCSY: Transverse rotating-frame Overhauser effect spectroscopy. *J. Am. Chem. Soc. 114*, 3157–3159.
27. Hwang, T. L., and Shaka, A. J. (1993) Reliable two-dimensional rotating-frame cross-relaxation measurements in coupled spin systems. *J. Magn. Reson., Ser. B 102*, 155–165.
28. Heck, M., Schädel, S. A., Maretzki, D., Bartl, F. J., Ritter, E., Palczewski, K., and Hofmann, K. P. (2003) Signaling states of rhodopsin. Formation of the storage form, metarhodopsin III, from active metarhodopsin II. *J. Biol. Chem. 278*, 3162–3169.
29. Güntert, P., Braun, W., and Wüthrich, K. (1991) Efficient computation of three-dimensional protein structures in solution from nuclear magnetic resonance data using the program DIANA and the supporting programs CALIBA, HABAS and GLOMSA. *J. Mol. Biol. 217*, 517–530.
30. Wüthrich, K. (1986) NMR of proteins and nucleic acids , John Wiley & Sons, New York.
31. Schwieters, C. D., Kuszewski, J. J., Tjandra, N., and Clore, G. M. (2003) The Xplor-NIH NMR molecular structure determination package. *J. Magn. Reson. 160*, 65–73.
32. Nilges, M. (1995) Calculation of protein structures with ambiguous distance restraints. Automated assignment of ambiguous NOE crosspeaks and disulphide connectivities. *J. Mol. Biol. 245*, 645–660.

33. Nilges, M., Kuszewski, J., and Brünger, A. T. (1991) Sampling properties of simulated annealing and distance geometry. In Computational aspects of the study of biological macromolecules by nuclear magnetic resonance spectroscopy (Hoch, J. C., Ed.) pp 451−455, Plenum Press, New York.
34. Parkes, J. H., Gibson, S. K., and Liebman, P. A. (1999) Temperature and pH dependence of the metarhodopsin I-metarhodopsin II equilibrium and the binding of metarhodopsin II to G protein in rod disk membranes. *Biochemistry 38*, 6862–6878.
35. Hofmann, K. P. (1985) Effect of GTP on the rhodopsin-G-protein complex by transient formation of extra metarhodopsin II. *Biochim. Biophys. Acta 810*, 278–281.
36. Ernst, O. P., Bieri, C., Vogel, H., and Hofmann, K. P. (2000) Intrinsic biophysical monitors of transducin activation: Fluorescence, UV-visible spectroscopy, light scattering, and evanescent field techniques. *Methods Enzymol. 315*, 471–489.
37. Pulvermüller, A., Maretzki, D., Rudnicka-Nawrot, M., Smith, W. C., Palczewski, K., and Hofmann, K. P. (1997) Functional differences in the interaction of arrestin and its splice variant, p44, with rhodopsin. *Biochemistry 36*, 9253–9260.
38. Pulvermüller, A., Palczewski, K., and Hofmann, K. P. (1993) Interaction between photoactivated rhodopsin and its kinase: Stability and kinetics of complex formation. *Biochemistry 32*, 14082–14088.
39. Heck, M., and Hofmann, K. P. (1993) G-protein-effector coupling: A real-time light-scattering assay for transducin-phosphodiesterase interaction. *Biochemistry 32*, 8220–8227.
40. Koenig, B. W., Kontaxis, G., Mitchell, D. C., Louis, J. M., Litman, B. J., and Bax, A. (2002) Structure and orientation of a G protein fragment in the receptor bound state from residual dipolar couplings. *J. Mol. Biol. 322*, 441–461.
41. Lovell, S. C., Davis, I. W., Arendall, W. B.III, de Bakker, P. I., Word, J. M., Prisant, M. G., Richardson, J. S., and Richardson, D. C. (2003) Structure validation by Cα geometry: $\phi$,$\psi$ and C$\beta$ deviation. *Proteins 50*, 437–450.
42. Kabsch, W., and Sander, C. (1983) Dictionary of protein secondary structure: Pattern recognition of hydrogen-bonded and geometrical features. *Biopolymers 22*, 2577–2637.
43. Altenbach, C., Yang, K., Farrens, D. L., Farahbakhsh, Z. T., Khorana, H. G., and Hubbell, W. L. (1996) Structural features and light-dependent changes in the cytoplasmic interhelical E-F loop region of rhodopsin: A site-directed spin-labeling study. *Biochemistry 35*, 12470–12478.
44. Farrens, D. L., Altenbach, C., Yang, K., Hubbell, W. L., and Khorana, H. G. (1996) Requirement of rigid-body motion of transmembrane helices for light activation of rhodopsin. *Science 274*, 768–770.
45. Williams, R. W., Chang, A., Juretic, D., and Loughran, S. (1987) Secondary structure predictions and medium range interactions. *Biochim. Biophys. Acta 916*, 200–204.
46. Albrand, J. P., Birdsall, B., Feeney, J., Roberts, G. C. K., and Burgen, A. S. V. (1979) The use of transferred nuclear Overhauser effects in the study of the conformations of small molecules bound to proteins. *Int. J. Biol. Macromol. 1*, 37–41.
47. Clore, G. M., and Gronenborn, A. M. (1982) Theory and application of the transferred nuclear Overhauser effect to the study of the conformations of small ligands bound to proteins. *J. Magn. Reson. 48*, 402–417.
48. Clore, G. M., and Gronenborn, A. M. (1983) Theory of the time dependent transferred nuclear Overhauser effect: Applications to structural analysis of ligand-protein complexes in solution. *J. Magn. Reson. 53*, 423–442.
49. Ni, F. (1994) Recent developments in transferred NOE methods. *Prog. NMR Spectrosc. 26*, 517–606.
50. Post, C. B. (2003) Exchange-transferred NOE spectroscopy and bound ligand structure determination. *Curr. Opin. Struct. Biol. 13*, 581–588.
51. Dratz, E. A., Furstenau, J. E., Lambert, C. G., Thireault, D. L., Rarick, H., Schepers, T., Pakhlevaniants, S., and Hamm, H. E. (1993) NMR structure of a receptor-bound G-protein peptide. *Nature 363*, 276–281.
52. Kisselev, O. G., Kao, J., Ponder, J. W., Fann, Y. C., Gautam, N., and Marshall, G. R. (1998) Light-activated rhodopsin induces structural binding motif in G protein α subunit. *Proc. Natl. Acad. Sci. U.S.A. 95*, 4270–4275.
53. Kisselev, O. G., McDowell, J. H., and Hargrave, P. A. (2004) The arrestin-bound conformation and dynamics of the phosphorylated carboxy-terminal region of rhodopsin. *FEBS Lett. 564*, 307–311.
54. Kisselev, O. G., Downs, M. A., McDowell, J. H., and Hargrave, P. A. (2004) Conformational changes in the phosphorylated C-terminal domain of rhodopsin during rhodopsin arrestin interactions. *J. Biol. Chem. 279*, 51203–51207.
55. Bakshi, K., Mercier, R. W., and Pavlopoulos, S. (2007) Interaction of a fragment of the cannabinoid CB1 receptor C-terminus with arrestin-2. *FEBS Lett. 581*, 5009–5016.
56. Kisselev, O. G., and Downs, M. A. (2003) Rhodopsin controls a conformational switch on the transducin $\gamma$ subunit. *Structure 11*, 367–373.
57. Park, J. H., Scheerer, P., Hofmann, K. P., Choe, H. W., and Ernst, O. P. (2008) Crystal structure of the ligand-free G-protein-coupled receptor opsin. *Nature 454*, 183–187.
58. Scheerer, P., Park, J. H., Hildebrand, P. W., Kim, Y. J., Krauss, N., Choe, H. W., Hofmann, K. P., and Ernst, O. P. (2008) Crystal structure of opsin in its G-protein-interacting conformation. *Nature 455*, 497–502.
59. Lange, O. F., Lakomek, N. A., Fares, C., Schröder, G. F., Walter, K. F., Becker, S., Meiler, J., Grubmüller, H., Griesinger, C., and de Groot, B. L. (2008) Recognition dynamics up to microseconds revealed from an RDC-derived ubiquitin ensemble in solution. *Science 320*, 1471–1475.
60. Modzelewska, A., Filipek, S., Palczewski, K., and Park, P. S. (2006) Arrestin interaction with rhodopsin: Conceptual models. *Cell Biochem. Biophys. 46*, 1–15.
61. Hanson, S. M., Gurevich, E. V., Vishnivetskiy, S. A., Ahmed, M. R., Song, X., and Gurevich, V. V. (2007) Each rhodopsin molecule binds its own arrestin. *Proc. Natl. Acad. Sci. U.S.A. 104*, 3125–3128.
62. Hanson, S. M., Van Eps, N., Francis, D. J., Altenbach, C., Vishnivetskiy, S. A., Arshavsky, V. Y., Klug, C. S., Hubbell, W. L., and Gurevich, V. V. (2007) Structure and function of the visual arrestin oligomer. *EMBO J. 26*, 1726–1736.
63. Skegro, D., Pulvermüller, A., Krafft, B., Granzin, J., Hofmann, K. P., Büldt, G., and Schlesinger, R. (2007) N-Terminal and C-terminal domains of arrestin both contribute in binding to rhodopsin. *Photochem. Photobiol. 83*, 385–392.
64. Kraulis, P. J. (1991) MOLSCRIPT: A program to produce both detailed and schematic plots of protein structures. *J. Appl. Crystallogr. 24*, 946–950.
65. Merritt, E. A., and Murphy, M. E. (1994) Raster3D Version 2.0. A program for photorealistic molecular graphics. *Acta Crystallogr. D50*, 869–873.